How to predict the ideal glass transition density in polydisperse hard-sphere packings

Vasili Baranau and Ulrich Tallarek

Citation: The Journal of Chemical Physics **143**, 044501 (2015); doi: 10.1063/1.4927077
View online: http://dx.doi.org/10.1063/1.4927077
View Table of Contents: http://scitation.aip.org/content/aip/journal/jcp/143/4?ver=pdfcov
Published by the AIP Publishing

How to predict the ideal glass transition density in polydisperse hard-sphere packings

Vasili Baranau and Ulrich Tallarek[a)]
Department of Chemistry, Philipps-Universität Marburg, Hans-Meerwein-Strasse 4, 35032 Marburg, Germany

(Received 28 April 2015; accepted 8 July 2015; published online 22 July 2015)

The formula for the entropy s of the accessible volume of the phase space for frictionless hard spheres is combined with the Boublík–Mansoori–Carnahan–Starling–Leland (BMCSL) equation of state for polydisperse three-dimensional packings to obtain an analytical expression for s as a function of packing density φ. Polydisperse hard-sphere packings with log-normal, Gaussian, and Pareto particle diameter distributions are generated to estimate their ideal glass transition densities φ_g. The accessible entropy s at φ_g is almost the same for all investigated particle diameter distributions. We denote this entropy as s_g and can predict φ_g for an arbitrary particle diameter distribution through an equation $s(\varphi) = s_g$. If the BMCSL equation of state is used for $s(\varphi)$, then φ_g is found to depend only on the first three moments of a particle diameter distribution. © *2015 AIP Publishing LLC.* [http://dx.doi.org/10.1063/1.4927077]

I. INTRODUCTION

The nature of the glass transition has been gaining significant attention over the past decades.[1–6] An important concept that emerged from the studies of glass dynamics is that of the ideal glass transition.[5,7–13] The latter is usually determined by the jump of compressibility or divergent alpha-relaxation time.[5,7–9] One of the simplest models that exhibits many interesting and important properties of real atomic, molecular, and colloidal systems, including glassy dynamics, is packings of frictionless hard spheres.[5,14,15] It is generally believed that the phase space of hard spheres becomes non-ergodic at the ideal glass transition density φ_g.[8,11]

In this paper, we derive an expression to predict φ_g for polydisperse packings of frictionless hard spheres. We combine the formula for the excess "liquid" entropy of frictionless hard-sphere packings[16,17] with the Boublík–Mansoori–Carnahan–Starling–Leland (BMCSL) equation of state for polydisperse three-dimensional hard spheres.[18–20] Thus, we obtain an analytical equation for the hard-sphere entropy *vs.* packing density. We assume that the entropy per particle at the ideal glass transition does not depend on the particle diameter distribution if the number of particles is large enough. When the critical value of the entropy per particle at φ_g is known, it is possible to estimate φ_g for packings with arbitrary particle diameter distribution: We need to find a density at which the entropy per particle equals the critical value. The resulting equation implies that φ_g shall depend only on the first three moments of a particle diameter distribution. Recent studies suggest that another characteristic density of frictionless hard-sphere packings, the J-point,[21] also depends only on the first three moments of the particle diameter distributions.[22,23]

The paper is structured as follows. In Section II, we derive the formula for the entropy *vs.* packing density and the master equation for estimating φ_g. In Section III, we generate three-dimensional frictionless hard-sphere packings with log-normal, Gaussian, and Pareto diameter distributions and estimate their ideal glass transition densities. In Section IV, we demonstrate that packing entropy from Section II at the estimated φ_g does not noticeably depend on the particle diameter distribution. Then, we demonstrate how well our predictions for φ_g compare to the estimates from simulations. Finally, we build a map of the ideal glass transition densities *vs.* the particle diameter standard deviation and skewness, provided that the mean particle diameter is unity.

II. THEORY

A. Packing entropy

Each configuration of hard spheres with predefined diameters corresponds to a point in the phase space for these spheres. At any solid volume density $\varphi > 0$, some points in the phase space correspond to configurations with particle intersections and are inaccessible, the others correspond to valid packing configurations and form the accessible part of the phase space. If the accessible phase space is still ergodic at a given density φ, it is possible to explicitly derive its volume V_{acc}.[16,17] If under packing entropy S we understand the logarithm of V_{acc}, $S = \ln(V_{\text{acc}})$, we obtain from Eq. (7) in Asenjo *et al.*,[16]

$$S(\varphi) = N \ln(V_{\text{box}}) - N \int_0^{\varphi} \frac{Z(\varphi') - 1}{\varphi'} \, \mathrm{d}\varphi', \qquad (1)$$

where V_{box} is the volume of the box in which the particles reside, $Z(\varphi)$ is the reduced kinematic pressure (compressibility factor), and N is the number of particles. Here, S is a total entropy, i.e., it includes both configurational and vibrational contributions. It is convenient to renormalize entropies and discard the $N \ln(V_{\text{box}})$ term, as well as to work with entropies per particle, i.e., divide entropy values by N. We refer to this

a)Electronic mail: tallarek@staff.uni-marburg.de

renormalized entropy per particle as s. Formally,

$$s(\varphi) = -\int_0^{\varphi} \frac{Z(\varphi') - 1}{\varphi'} \mathrm{d}\varphi'. \quad (2)$$

B. Equation of state

The phase space for hard spheres is believed to become non-ergodic at the ideal glass transition density φ_g.[8,24] Thus, Eq. (1) is applicable for $\varphi \le \varphi_g$. A common equation of state utilized for polydisperse hard spheres is the so-called BMCSL equation of state.[18–20] Berthier and Witten showed[9] that this equation of state successfully predicts reduced pressure in equilibrated bidisperse hard-sphere packings up to a very high density 0.597, though different techniques they used predicted φ_g at different densities, from 0.592 to 0.635. In our previous paper,[24] we confirmed that this equation of state predicts pressure in equilibrated hard-sphere packings with log-normal particle diameter distribution for $\varphi \le \varphi_g$, if the packings do not exhibit spontaneous crystallization. We assume that this equation of state is applicable up to the ideal glass transition for equilibrated packings with any diameter distribution. Thus, we may complement Eq. (1) with the specification of the reduced pressure $Z(\varphi)$. When we apply the BMCSL equation of state to packings that exhibit spontaneous crystallization, we imply that crystal-like configurations are excluded from the phase space. As long as we operate only in the range of densities $\varphi \le \varphi_g$, we do not require any assumptions about the pressure behaviour for $\varphi > \varphi_g$.

We use the following representation of the BMCSL equation of state (Eq. (9) in Ogarko and Luding[20]):

$$Z(\varphi) = \frac{1}{1-\varphi} + O_1 \frac{3\varphi}{(1-\varphi)^2} + O_2 \frac{\varphi^2(3-\varphi)}{(1-\varphi)^3}, \quad (3)$$

where $O_1 = \frac{\langle r\rangle\langle r^2\rangle}{\langle r^3\rangle}$, $O_2 = \frac{\langle r^2\rangle^3}{\langle r^3\rangle^2}$, and $\langle r^i\rangle$ is the ith raw moment of particle radii r. Eq. (2) then becomes

$$s(\varphi) = 3O_1 - (O_2 - 1)\ln(1-\varphi) - \frac{(O_2 - 3O_1)\varphi + 3O_1}{(1-\varphi)^2}. \quad (4)$$

For monodisperse packings, $O_1 = 1$ and $O_2 = 1$.

Below, we use the particle diameter relative standard deviation (polydispersity) σ and the particle diameter skewness γ. Here, $\sigma = \sqrt{\langle \Delta d^2\rangle}/\langle d\rangle = \sqrt{\langle \Delta r^2\rangle}/\langle r\rangle$ and $\gamma = \langle \Delta d^3\rangle / \langle \Delta d^2\rangle^{3/2} = \langle \Delta r^3\rangle / \langle \Delta r^2\rangle^{3/2}$, where d is the particle diameter. The relation between the parameter sets (O_1, O_2) and (σ, γ) is as follows:

$$\sigma^2 = \frac{O_2}{O_1^2} - 1, \gamma = \frac{1}{\sigma^3}\left[\frac{O_2}{O_1^3} - 3\frac{O_2}{O_1^2} + 2\right], \quad (5a)$$

$$O_1 = \frac{\sigma^2 + 1}{\gamma\sigma^3 + 3\sigma^2 + 1}, O_2 = \frac{(\sigma^2+1)^3}{(\gamma\sigma^3 + 3\sigma^2 + 1)^2}. \quad (5b)$$

C. Equal entropies at the ideal glass transition

We assume that the fraction of the inaccessible phase space at which the phase space becomes non-ergodic does not depend on the particle diameter polydispersity, if the packings contain the same large enough number of particles N. It means that the entropy at the ideal glass transition is the same for all polydispersities at a given large enough N. This assumption will be verified later for computer-generated packings. We refer to the renormalized entropy per particle at the ideal glass transition in the thermodynamic limit as s_g. To predict φ_g for an arbitrary particle size distribution, we need to find such a φ that $s(\varphi) = s_g$. Thus, we arrive at the master equation

$$3O_1 - (O_2 - 1)\ln(1-\varphi) - \frac{(O_2 - 3O_1)\varphi + 3O_1}{(1-\varphi)^2} = s_g. \quad (6)$$

Instead of s_g, we can parametrize Eq. (6) with φ_g of a reference particle diameter distribution. Then, we can compute s_g via Eq. (4).

III. IDEAL GLASS TRANSITION DENSITIES FROM SIMULATIONS

In our previous paper,[24] we estimated the ideal glass transition densities φ_g for particles with log-normal diameter distributions having relative diameter standard deviations σ from 0.05 to 0.3 in steps of 0.05. We repeated the procedure from that paper to determine φ_g for packings with (truncated) Gaussian and Pareto diameter distributions (cf. Table I). Gaussian and Pareto distributions also had relative diameter standard deviations σ from 0.05 to 0.3 in steps of 0.05. Now we briefly describe the procedure from that paper.[24]

A. Definitions

In the following discussion, we rely on the concepts of jamming[14,25–27] and inherent structures.[28–30] To introduce them, we need two types of packing descriptions. We assume that certain nominal particle diameters are always specified for a packing and that actual particle diameters shall be proportional to the nominal ones and are thus determined by the proportionality ratio or by the packing density φ. We also define $\vec{x}$ as a hypervector in the phase space formed by $3(N-1)$ particle coordinates. A packing description needed to define jamming and assumed everywhere outside this subsection specifies both $\vec{x}$ and φ (particle positions and actual diameters); thus, we denote it as $(\vec{x}, \varphi)$. A packing description needed to define inherent structures specifies only particle positions $\vec{x}$ but not the packing density φ (actual particle diameters).

A set of particles $(\vec{x}, \varphi)$ with predefined actual diameters is called jammed, if there exists no combination of particle displacements that avoids particle intersections, except for shifts or rotations of the system as a whole. A packing is called jammed if there is a subset of particles that is jammed. Inherent structures were initially introduced for systems with a soft potential,[28,29] which are described only by $\vec{x}$. For such systems, an inherent structure is by definition a packing configuration $\vec{x}_0$ with a local potential energy minimum in the phase space. For hard-sphere packings, the potential energy $U(\vec{x})$ at a given configuration $\vec{x}$ is replaced by the maximum packing density achievable at this configuration taken with the minus sign, $U(\vec{x}) = -\varphi_{\max}(\vec{x})$. The maximum density $\varphi_{\max}(\vec{x})$ for given particle positions $\vec{x}$ is computed by "inflating" particles

TABLE I. Properties of the different particle diameter distributions used in the text.

Distribution	Probability density function	Important moments	Skewness γ *vs.* polydispersity σ
Truncated Gaussian[a]	$f_G(x;\mu_G,\sigma_G) = C\frac{1}{\sigma_G\sqrt{2\pi}}e^{-\frac{(x-\mu_G)^2}{2\sigma_G^2}}, x \geq 0,$ $C = 2\left(1-\mathrm{erf}\left(\frac{x-\mu_G}{\sigma_G\sqrt{2}}\right)\right)^{-1}$	$\langle x\rangle \approx \mu_G,$ $\langle \Delta x^2\rangle \approx \sigma_G^2,$ $\langle \Delta x^3\rangle \approx 0$	$\gamma \approx 0$
Log-normal	$f_{LN}(x;\mu_{LN},\sigma_{LN}) = \frac{1}{x\sigma_{LN}\sqrt{2\pi}}e^{-\frac{(\ln(x)-\mu_{LN})^2}{2\sigma_{LN}^2}},$ $x > 0$	$\langle x\rangle = e^{\mu_{LN}+\sigma_{LN}^2/2},$ $\langle \Delta x^2\rangle = \langle x\rangle^2(e^{\sigma_{LN}^2}-1),$ $\gamma = (e^{\sigma_{LN}^2}+2)\sqrt{e^{\sigma_{LN}^2}-1}$	$\gamma = (\sigma^2+3)\sigma$
Pareto	$f_P(x;x_m,\alpha) = \frac{\alpha x_m^\alpha}{x^{\alpha+1}},$ $x \geq x_m$	$\langle x^i\rangle = \begin{cases}\frac{\alpha x_m^i}{\alpha-i}, & \text{if } \alpha > i\\ \infty, & \text{if } \alpha \leq i\end{cases}$	$\gamma = \begin{cases}2\sigma\frac{A+2}{A-2}(A-1), & \text{if } \sigma < \frac{1}{\sqrt{3}} \approx 0.577\\ \infty, & \text{if } \sigma \geq \frac{1}{\sqrt{3}} \approx 0.577\end{cases},$ where $A = \sqrt{1+\frac{1}{\sigma^2}}$

[a]The truncated Gaussian distribution, in general, has moments different from the usual (untruncated) Gaussian distribution. But the widest distribution $f_G(x;\mu_G,\sigma_G)$ used in our simulations, with $\mu_G = 1$ and $\sigma_G = 0.3$, has $\langle x\rangle \approx 1.0005$ and $\sqrt{\langle \Delta x^2\rangle} \approx 0.2992$. Therefore, in this table, we neglect for simplicity corrections to moments stemming from the truncation of values at $x = 0$.

so that their diameters remain proportional to the nominal values until at least one pair of particles develops a contact. When we talk about a density of an inherent structure $\vec{x}_0$, we assume $\varphi_{\max}(\vec{x}_0)$. It can be shown that inherent structures correspond to jammed configurations and, vice versa, jammed configurations correspond to inherent structures. For example, let a packing reside in an inherent structure $\vec{x}_0$ and let the particle diameters be maximally possible for these particle positions $\vec{x}_0$ ($\varphi = \varphi_{\max}(\vec{x}_0)$). As far as an inherent structure corresponds to a local density maximum, any infinitesimal change in particle positions from the current configuration $(\vec{x}_0, \varphi_{\max}(\vec{x}_0))$ will result in particle intersections and thus is forbidden. This implies that any inherent structure $\vec{x}_0$ corresponds to a jammed configuration $(\vec{x}_0, \varphi_{\max}(\vec{x}_0))$.

To any configuration $\vec{x}$, we can apply a steepest descent in the potential energy landscape $U(\vec{x})$ (infinitely fast quench, Stillinger quench) and reach a certain inherent structure $\vec{x}_{CJ}$. In this way, the entire phase space can be split into basins of attraction of inherent structures. Thus, an inherent structure $\vec{x}_{CJ}$ corresponds to the "closest jammed configuration" $(\vec{x}_{CJ}, \varphi_{\max}(\vec{x}_{CJ}))$ for configurations $\vec{x}$ in the basin of attraction of this structure. The density of this configuration $\varphi_{CJ} = \varphi_{\max}(\vec{x}_{CJ})$ is thus the "closest jamming density" for configurations $\vec{x}$ in the corresponding basin of attraction. As mentioned in Section II A, at any given packing density φ, certain regions of the phase space will be unavailable. We refer to an intersection of a basin of attraction and the available part of the phase space as a "bounding region." Mathematically, precise definitions of inherent structures, basins of attraction, and bounding regions can be found in our previous paper.[31]

At a given packing density φ, bounding regions with a certain jamming density φ_{CJ} will dominate the phase space. We refer to their jammed configurations $(\vec{x}_{CJ}, \varphi_{\max}(\vec{x}_{CJ}) = \varphi_{CJ})$ as "dominant jammed configurations" and denote their jamming density as a "dominant jamming density" φ_{DJ}.[24] If we take an arbitrary packing $(\vec{x}, \varphi)$ at a given density φ and let it equilibrate (undergo molecular dynamics with zero compression rate), the packing will eventually reach one of the dominant bounding regions, given that the phase space is still ergodic at this density. If the phase space is non-ergodic (formed by disconnected regions), its separate parts will be dominated by different bounding regions. In this case, the closest jamming density of a packing after equilibration will depend on the initial configuration $\vec{x}$.

B. Simulation procedure

The idea of our method for determination of the ideal glass transition densities φ_g is to generate packings in a wide range of densities φ, equilibrate them, and search for inherent structures of these equilibrated packings. The densities of these inherent structures are the dominant jamming densities φ_{DJ}. By definition, φ_g is a density where the phase space becomes disjoint and non-ergodic. It is believed that the plot φ_{DJ} *vs.* φ for a given particle diameter distribution reaches its maximum at $\varphi = \varphi_g$ if crystallization is suppressed.[5,7–9]

First, we computationally generated packings of 10^4 particles in three-dimensional fully periodic boxes in a wide range of densities (e.g., for Pareto packings with $\sigma = 0.05$, $\varphi = 0.4 - 0.653$) using the force-biased algorithm.[32,33] The lowest contraction rate for the algorithm was 10^{-7}. It ensures that the largest density of the packings is close to the maximum possible density for a given diameter distribution (the glass close packing limit φ_{GCP}).[5]

Second, we equilibrated the generated packings, i.e., conducted simulations using the Lubachevsky–Stillinger algorithm[34,35] with zero compression rate until the kinematic pressure became stationary. We equilibrate the packings by performing sets of 2×10^7 collisions with zero compression rate in a loop until the relative difference of reduced pressures between the last two sets is less than 10^{-4}, so that the pressure can be regarded as stationary. More precisely, to measure the pressure during the 2×10^7 collisions, we average pressures for 100 sub-sets of 2×10^5 collisions, which amounts

to 20 collisions in a sub-set per particle. We use our own implementation[36] of the Lubachevsky–Stillinger packing generation algorithm to carry out the equilibration.

Third, we searched for the inherent structure densities of the equilibrated packings φ_{DJ} using the modified Lubachevsky–Stillinger algorithm.[24,31,36] The modified algorithm starts from a compression with a high rate (=10) until the non-equilibrium reduced pressure is high enough (10^{12}); then, it reduces the compression rate by a factor of two and runs the simulation again until the pressure is high enough; this loop repeats until the compression rate is below 10^{-4}. The root mean square particle velocity was $\sqrt{3 \cdot 0.2}$. It corresponds to a packing temperature of 0.2, as far as we assigned unity mass to all the particles and set the Boltzmann constant to unity. Similar modifications have been used by other authors before.[7,30,37,38]

It is possible to get estimates of φ_{DJ} (which we will denote as φ_{DJE}) already from equilibrium pressures through the equation of state by Salsburg and Wood,[7,9,24,39] $\varphi_{DJE} = \varphi[1 + 1/(Z(\varphi) - 1)]^3$. This equation is derived under the free-volume approximation, which means that (i) during equilibration, particle centers cannot leave the Voronoi cells that correspond to the initial particle positions and (ii) particles move inside their Voronoi cells independently. Salsburg and Wood[39] derived another functionally similar equation for $\varphi_{DJE}(\varphi)$ under the assumptions that the current bounding region is small enough and closed (i.e., disconnected from other bounding regions). These two sets of assumptions are closely related.[39] We show the estimates φ_{DJE} *vs.* φ for Pareto packings in Fig. 1(a) (cf. Fig. 4 in Skoge *et al.*[7]).

Dominant jamming densities φ_{DJ} for Pareto packings are displayed in Fig. 1(b). We do not show the plots for Gaussian packings because they are qualitatively and quantitatively similar to the plots for the log-normal packings, which can be found in our previous paper.[24] The outburst in the $\varphi_{DJ}(\varphi)$ plot for $\sigma = 0.05$ corresponds to spontaneous partial crystallization.[5,7,8,40–42]

C. Analysis of dominant jamming densities

In Fig. 1, we depict the black dashed lines corresponding to $\varphi_{DJE} = \varphi$ (panel (a)) and $\varphi_{DJ} = \varphi$ (panel (b)). The plots for Pareto packings for each polydispersity approach these lines for large values of φ. This happens because at high φ the packings are close to jamming, i.e., the accessible parts of the basins of attraction where the packings reside are closed and small. This implies high equilibrium pressure[39] (and thus $\varphi_{DJE} \approx \varphi$). This also implies that (i) an initial basin of attraction is the only accessible one and (ii) an initial unjammed packing configuration at φ is close to the jammed configuration of this basin, which is automatically the dominant jammed configuration. Thus, $\varphi_{DJ} \approx \varphi$.

As mentioned, the plot φ_{DJ} *vs.* φ shall reach its maximum at $\varphi = \varphi_g$ if crystallization is suppressed. The dominant jamming density φ_{DJ} at $\varphi = \varphi_g$ corresponds to a lower boundary of the ideal glass density (the glass close packing limit φ_{GCP}). Additionally, the plateaus in the left part of Fig. 1(b) correspond to the J-segments, which are by definition density intervals where almost all Poisson packings will jam after searching for the closest jamming density (infinitely fast compression).[21,43,44] It is believed that the J-segments converge to their upper boundaries in the thermodynamic limit.[21] These upper boundaries are referred to as J-points φ_J. Fig. 1(b) mostly corresponds to the "many glassy states" model[5,9] and can be mapped to Fig. 7 in Berthier and Witten[9] and Fig. 4(a) in Parisi and Zamponi.[5] For example, φ_{th}, φ_K, and φ_{GCP} in Fig. 4(a) in Parisi and Zamponi[5] map to φ_J, φ_g, and φ_{GCP}, respectively, from this paper.

Fig. 1(a) recovers many features of Fig. 1(b), for example, the local maxima around $\varphi = \varphi_g$, the positions of φ_g, the presence of spontaneous crystallization, and proximity of packings to jamming for $\varphi \to \varphi_{GCP}$. At the same time, it does not reveal the plateau $\varphi_{DJ} = \varphi_J$ for low φ, because the preconditions for the equation of state of Salsburg and Wood are not satisfied for such low densities. Thus, Fig. 1 shows that the plot $\varphi_{DJE}(\varphi)$ alone shall be used carefully to analyse the structure of the phase space and should be accompanied by the $\varphi_{DJ}(\varphi)$ plot. We also point out a principal difference between the plots in Fig. 1(a) and the plots in Fig. 4 in Skoge *et al.*[7] and Figs. 2 and 3 in Ogarko and Luding.[20] These authors track pressures along a single compression and depict jamming density estimates during a single compression. For very slow compressions, these jamming density estimates can be treated as approximations of φ_{DJE}, because a sufficiently

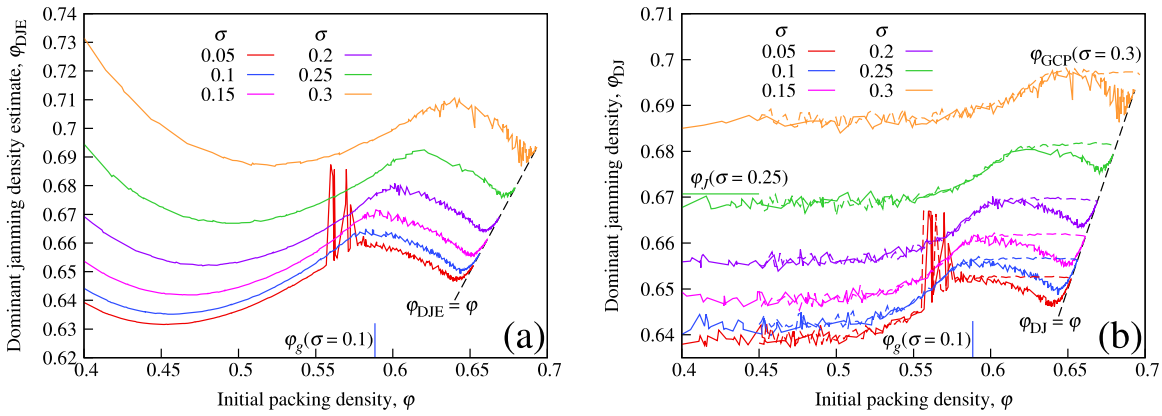

FIG. 1. Dominant jamming densities for Pareto packings. (a) Estimates of dominant jamming densities through the Salsburg–Wood equation of state. (b) Dominant jamming densities obtained through the modified Lubachevsky–Stillinger algorithm. Particle diameter relative standard deviations σ are provided in the legends. Coloured dashed lines denote dominant jamming densities for diluted densest packings of the corresponding particle diameter distribution.

slow compression can "equilibrate" the packing before the packing density (and thus the structure of the phase space) is changed significantly.

D. Diluted densest packings

To demonstrate that the maxima in the $\varphi_{DJ}(\varphi)$ plots (solid lines, Fig. 1(b)) mark the onset of non-ergodicity, we generated another set of packings and searched for their dominant jamming densities. First, we chose for each σ a reference packing, a packing with φ_{DJ} close to φ_{GCP}. For $\sigma = 0.05 - 0.2$, we took the dominant jammed packing at the maximum initial density (the right-most point in Fig. 1(b)). For $\sigma = 0.25 - 0.3$, we used the dominant jammed packing with maximum jammed density (the highest point in Fig. 1(b)). Then, we scaled the particle positions so that we obtained packings with exactly the same particle diameters but with densities in the range $[0.4, \varphi_{GCP})$. Finally, we determined the dominant jamming densities φ_{DJ} for these scaled packings, as done in Section III B above. We refer to these scaled packings as "diluted densest" ones. We show the plots φ_{DJ} *vs.* φ for these packings as dashed lines of the corresponding colour in Fig. 1(b). The $\varphi_{DJ}(\varphi)$ plots of the force-biased Pareto packings and the diluted densest Pareto packings with the same σ start to deviate approximately at the maxima of the plots for the force-biased packings (solid lines in Fig. 1(b)); the deviation signals the onset of non-ergodicity around the maxima. The diluted densest packings (dashed lines in Fig. 1(b)) also have $\varphi_{DJ} \approx \varphi_{GCP}$ for densities φ higher than the positions of the mentioned maxima on the X-axis. The plots for $\varphi_{DJ}(\varphi)$ for Gaussian packings created with the force-biased algorithm and diluted densest Gaussian packings look qualitatively the same as in Fig. 1(b).

E. Determination of the ideal glass transition densities

For Pareto packings, the maxima of the $\varphi_{DJ}(\varphi)$ plots in Fig. 1(b) are blurred and we could not determine their positions reliably. To estimate φ_g for the Pareto packings, we determined the densities at the onset of the plateaus $\varphi_{DJ} \approx \varphi_{GCP}$ in the $\varphi_{DJ}(\varphi)$ plots for the diluted densest packings in Fig. 1(b) (the dashed lines). More precisely, each dashed line in Fig. 1(b) comprises of three distinct sections: a plateau $\varphi_{DJ} \approx \varphi_J$ in the left part of the figure, a plateau $\varphi_{DJ} \approx \varphi_{GCP}$ in the right part of the figure, and an increase between the two plateaus. Thus, to estimate φ_g for the Pareto packings, we determined the average φ_{DJ} values of the six plateaus $\varphi_{DJ} \approx \varphi_{GCP}$ in the right part of Fig. 1(b). Then, we fitted the increasing parts of each curve between the plateaus with second-order polynomials. Finally, we tracked the points of intersections of these polynomials with the corresponding plateaus $\varphi_{DJ} \approx \varphi_{GCP}$. For $\sigma = 0.05$, we excluded points corresponding to spontaneous crystallization. For Gaussian packings, we estimated φ_g by direct detection of the maxima in the $\varphi_{DJ}(\varphi)$ plots for the force-biased algorithm, as we have done for the log-normal packings.[24] This is possible, because the maxima in the $\varphi_{DJ}(\varphi)$ plots are pronounced for these particle diameter distributions.

TABLE II. Ideal glass transition densities φ_g for the log-normal, Gaussian, and Pareto particle diameter distributions *vs.* different particle diameter relative standard deviations σ.

σ	0.05	0.1	0.15	0.2	0.25	0.3
Log-normal	0.586	0.59	0.595	0.602	0.61	0.622
Gaussian	0.587	0.59	0.594	0.601	0.61	0.617
Pareto	0.586	0.588	0.596	0.604	0.620	0.640

The ideal glass transition densities for the particle size distributions under consideration are presented in Table II. Fig. 1(b) allows to estimate two more characteristic densities of the packings. As mentioned, one can estimate the lower boundary of φ_{GCP} by taking φ_{DJ} at $\varphi = \varphi_g$[24] and φ_J by taking the upper boundary of the plateaus in the left part of the figure. For reference, we present φ_J and φ_{GCP} for the Gaussian and Pareto particle diameter distributions in Table III. The data for the log-normal packings can be found in Table 4 in our previous paper[31] and are included in Table III for convenience.

IV. RESULTS AND DISCUSSION

A. Ideal glass transition entropies from simulations

We determined entropies per particle at the ideal glass transition $s(\varphi_g)$ for the polydisperse packings under study. Eq. (2) was used with two types of pressure: (i) spline-interpolated equilibrium pressure from simulations and (ii) the BMCSL pressure from Eq. (3) (cf. Eq. (4)). We depict the values of $s(\varphi_g)$ for the log-normal and Pareto packings in Fig. 2. Entropies for the Gaussian packings behave very similarly and are omitted for clarity. Fig. 2 shows that the entropies at the ideal glass transition do not significantly depend on the particle diameter distribution type and its parameters, which supports the assumption of equal entropies from Section II C. Fig. 2 also shows that the use of the BMCSL equation of state instead of real pressures leads to minute changes in the entropy estimates and thus will have negligible effect on the solution of the equation $s(\varphi) = s_g$. Indeed, let us denote with $Z_{sim}(\varphi)$ the equilibrium reduced pressure from the simulations and with $Z(\varphi)$, as earlier, the reduced pressure from the BMCSL equation of state, Eq. (3). Then, the relative pressure difference $\delta = |Z_{sim}(\varphi) - Z(\varphi)|/Z_{sim}(\varphi)$ becomes larger than 10^{-2} not earlier than for $\varphi = \varphi_g - 0.02$ and is never larger than 0.06 at $\varphi = \varphi_g$ for all the packing types under study (cf. Fig. 6 in our previous paper[24]).

TABLE III. J-point densities φ_J and ideal glass densities φ_{GCP} for the log-normal, Gaussian, and Pareto particle diameter distributions *vs.* different particle diameter relative standard deviations σ.

σ	0.05	0.1	0.15	0.2	0.25	0.3
Log-normal, φ_J	0.642	0.644	0.649	0.654	0.660	0.668
Log-normal, φ_{GCP}	0.653	0.655	0.661	0.665	0.672	0.679
Gaussian, φ_J	0.641	0.645	0.648	0.652	0.657	0.661
Gaussian, φ_{GCP}	0.652	0.656	0.661	0.667	0.671	0.674
Pareto, φ_J	0.642	0.645	0.650	0.659	0.671	0.689
Pareto, φ_{GCP}	0.654	0.658	0.663	0.671	0.680	0.697

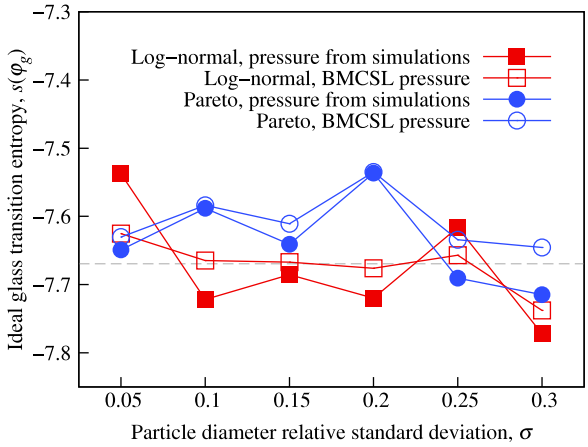

FIG. 2. Ideal glass transition entropies for the log-normal and Pareto particle diameter distributions (cf. Eq. (2)). The dashed grey line denotes the value used in Eq. (6).

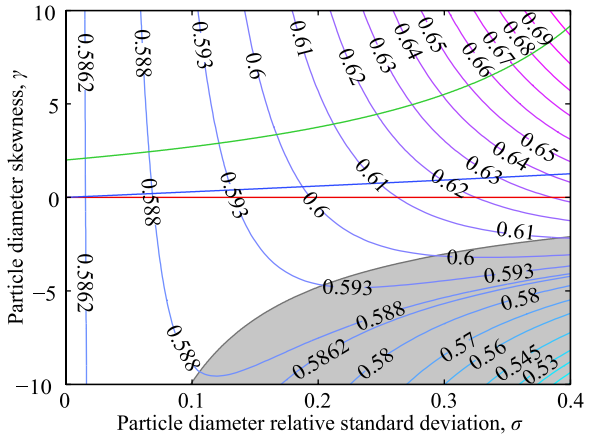

FIG. 4. Ideal glass transition density map. Red, blue, and green lines correspond to the Gaussian, log-normal, and Pareto particle diameter distributions, respectively.

B. Comparison of theory and simulations

We chose the value of s_g to minimize the error for the log-normal distribution,[24] i.e., between φ_g from the simulations (Table II) and φ_g from theory (Eq. (6)). This led to $s_g = -7.6693$, if the natural logarithm is used for the entropy, and is indicated by the dashed grey line in Fig. 2. As mentioned, we can parametrize Eq. (6) with φ_g for a specific particle size distribution, producing s_g from Eq. (4). We use the monodisperse particle diameter distribution as a reference and denote the corresponding φ_g as φ_g^*. This approach assumes that crystallization is suppressed in monodisperse packings and pressure in these packings is described with the BMCSL equation of state for all $\varphi \le \varphi_g$. The obtained s_g corresponds to $\varphi_g^* = 0.5861$. We note that a naïve third-order polynomial fit of φ_g from simulations with the log-normal particle diameter distribution and its extrapolation on the monodisperse case gave $\varphi_g^* \approx 0.585$.[24]

We used the value $s_g = -7.6693$ ($\varphi_g^* = 0.5861$) to predict φ_g through Eq. (6) for all the packing types under study. The comparison between theoretical predictions and simulation results can be found in Fig. 3. The figure shows that Eq. (6) can successfully predict the ideal glass transition densities φ_g.

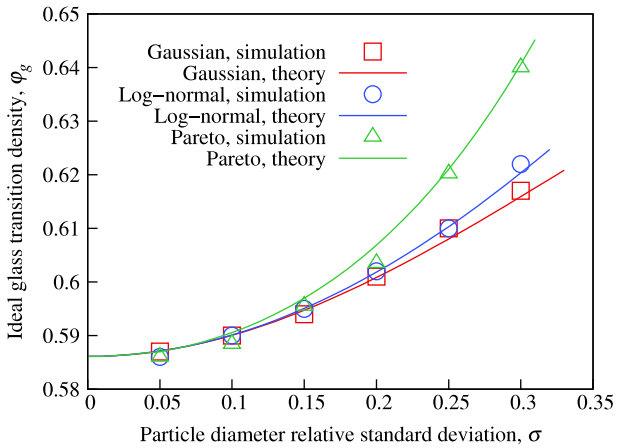

FIG. 3. Ideal glass transition densities from theory (cf. Eq. (6)) and simulations (cf. Fig. 1) for the log-normal, Gaussian, and Pareto particle diameter distributions.

C. Ideal glass transition density map

According to Eq. (6), the ideal glass transition densities shall depend only on the first three raw moments of the particle diameter distributions, if the BMCSL equation of state is used for the compressibility factor. As far as the mean diameter determines the length scale, we can present φ_g as a function of the particle diameter relative standard deviation σ and particle diameter skewness γ. In Fig. 4, we present φ_g for different values of these parameters. We also draw the lines that correspond to the log-normal, Gaussian, and Pareto distributions used in this paper. The analytical forms of these lines can be found in Table I. We note here that the results of recent studies suggest that the J-point density φ_J is also determined only by the first three moments of a particle diameter distribution.[22,23]

Ogarko and Luding[20] showed (cf. Appendix B of that paper) that for an arbitrary distribution with non-negative support the following property holds: $O_2 \le O_1$ (more generally, $0 \le O_1^2 \le O_2 \le O_1 \le 1$). In terms of skewness γ and polydispersity σ, $O_2 \le O_1$ means that $\gamma \ge \sigma - \frac{1}{\sigma}$, while the other inequalities are always satisfied. The inaccessible values of γ ($\gamma < \sigma - \frac{1}{\sigma}$,) are denoted in Fig. 4 with grey colour (shaded lower right corner). The beta and Kumaraswamy distributions, for example, can approach the line $\gamma = \sigma - \frac{1}{\sigma}$ arbitrary close.

Fig. 4 shows that distributions with higher skewness shall generally have higher ideal glass transition densities. At the same time, it is not obvious from Fig. 4 if there are values of σ and γ that correspond to $\varphi_g < \varphi_g^* = 0.5861$. Nevertheless, it is easy to determine a functional form of O_2 *vs.* O_1 that results in $\varphi_g = \varphi_g^*$: One has to substitute $\varphi_g = \varphi_g^*$ into Eq. (6), which will imply a linear dependence of O_2 *vs.* O_1 (omitted here for brevity). It can easily be verified that this critical line will intersect the line $O_2 = O_1$ (boundary of the grey zone in Fig. 4) only at $O_1 = 1$. The distribution with $O_1 = O_2 = 1$ is the monodisperse distribution. Thus, the monodisperse distribution possesses the lowest possible ideal glass transition density φ_g according to our model.

As stated in Table I, the skewness of the Pareto distribution diverges and becomes infinite at polydispersity $\sigma \approx 0.577$

(corresponding to the distribution parameter $\alpha = 3$). Infinite skewness implies that both O_1 and O_2 are zero (cf. Eq. (5b)). It follows from Eq. (6) that in this case $\varphi_g = 1 - e^{s_g} = 1 - e^{-7.6} \approx 1$. This result appears unrealistic and may be explained as follows: (i) Assumptions used to derive Eq. (6) are not applicable for such distributions; (ii) for such distributions, the ideal glass transition density φ_g is larger than the ideal glass density φ_{GCP}, so φ_g can never be reached and the phase space remains ergodic in the entire range of accessible densities up to φ_{GCP}; and (iii) φ_g is indeed close to unity and φ_{GCP} is (as usually) larger than φ_g, which implies that one can actually arrange particles in a packing to cover the entire packing space and reach unity density. There are two more critical values for the Pareto distribution parameter α, i.e., $\alpha = 2$ and $\alpha = 1$, at which the polydispersity and the mean particle diameter, respectively, become infinite. We assume that $\alpha \leq 2$ implies that both O_1 and O_2 can obtain any value in the range $[0, 1]$ depending on the current sample of particle diameters and φ_g can thus attain any value from its possible range. These special cases of the Pareto distribution parameters require separate investigation.

V. SUMMARY

In this paper, we combined the formula for the volume of the available phase space of frictionless hard spheres[16,17] with the BMCSL equation of state.[18,20] We thus obtained an analytical equation for the entropy s of frictionless polydisperse three-dimensional hard-sphere packings *vs.* the packing density φ. Through computer simulations, we estimated the ideal glass transition densities φ_g of packings with the log-normal, Gaussian, and Pareto particle diameter distributions. We discovered that the entropy at the estimated ideal glass transition densities does not significantly depend on the particle diameter distribution and presumably equals some characteristic value s_g. Thus, under the assumption of equal entropies at the ideal glass transition, we may predict the ideal glass transition density φ_g for an arbitrary particle diameter distribution by solving the equation $s(\varphi) = s_g$. According to this equation, φ_g shall depend only on the first three raw moments of the particle diameter distribution. We also provided a map of φ_g *vs.* particle diameter relative standard deviation and particle diameter skewness. This map may be used to design particle size distributions with desired values of φ_g. Our results help to understand the nature of the ideal glass transition and predict its properties in more complex atomic, molecular, or colloidal systems.

[1]J. H. Gibbs and E. A. DiMarzio, J. Chem. Phys. **28**, 373 (1958).
[2]G. Adam and J. H. Gibbs, J. Chem. Phys. **43**, 139 (1965).
[3]C. A. Angell, J. Phys. Chem. Solids **49**, 863 (1988).
[4]P. G. Debenedetti and F. H. Stillinger, Nature **410**, 259 (2001).
[5]G. Parisi and F. Zamponi, Rev. Mod. Phys. **82**, 789 (2010).
[6]G. L. Hunter and E. R. Weeks, Rep. Prog. Phys. **75**, 066501 (2012).
[7]M. Skoge, A. Donev, F. H. Stillinger, and S. Torquato, Phys. Rev. E **74**, 041127 (2006).
[8]E. Zaccarelli, C. Valeriani, E. Sanz, W. C. K. Poon, M. E. Cates, and P. N. Pusey, Phys. Rev. Lett. **103**, 135704 (2009).
[9]L. Berthier and T. A. Witten, Phys. Rev. E **80**, 021502 (2009).
[10]G. Brambilla, D. El Masri, M. Pierno, L. Berthier, L. Cipelletti, G. Petekidis, and A. B. Schofield, Phys. Rev. Lett. **102**, 085703 (2009).
[11]G. Pérez-Ángel, L. E. Sánchez-Díaz, P. E. Ramírez-González, R. Juárez-Maldonado, A. Vizcarra-Rendón, and M. Medina-Noyola, Phys. Rev. E **83**, 060501 (2011).
[12]T. Voigtmann, A. M. Puertas, and M. Fuchs, Phys. Rev. E **70**, 061506 (2004).
[13]G. Parisi and F. Zamponi, J. Chem. Phys. **123**, 144501 (2005).
[14]S. Torquato and F. H. Stillinger, Rev. Mod. Phys. **82**, 2633 (2010).
[15]V. Ogarko, N. Rivas, and S. Luding, J. Chem. Phys. **140**, 211102 (2014).
[16]D. Asenjo, F. Paillusson, and D. Frenkel, Phys. Rev. Lett. **112**, 098002 (2014).
[17]D. Frenkel and A. J. C. Ladd, J. Chem. Phys. **81**, 3188 (1984).
[18]T. Boublík, J. Chem. Phys. **53**, 471 (1970).
[19]G. A. Mansoori, N. F. Carnahan, K. E. Starling, and T. W. Leland, J. Chem. Phys. **54**, 1523 (1971).
[20]V. Ogarko and S. Luding, J. Chem. Phys. **136**, 124508 (2012).
[21]C. S. O'Hern, L. E. Silbert, A. J. Liu, and S. R. Nagel, Phys. Rev. E **68**, 011306 (2003).
[22]A. Santos, S. B. Yuste, M. López de Haro, G. Odriozola, and V. Ogarko, Phys. Rev. E **89**, 040302 (2014).
[23]K. W. Desmond and E. R. Weeks, Phys. Rev. E **90**, 022204 (2014).
[24]V. Baranau and U. Tallarek, Soft Matter **10**, 7838 (2014).
[25]A. Donev, J. Appl. Phys. **95**, 989 (2004).
[26]A. Donev, S. Torquato, F. H. Stillinger, and R. Connelly, J. Comput. Phys. **197**, 139 (2004).
[27]A. Donev, F. H. Stillinger, and S. Torquato, J. Chem. Phys. **127**, 124509 (2007).
[28]F. H. Stillinger, E. A. DiMarzio, and R. L. Kornegay, J. Chem. Phys. **40**, 1564 (1964).
[29]F. H. Stillinger, Science **267**, 1935 (1995).
[30]S. Torquato and Y. Jiao, Phys. Rev. E **82**, 061302 (2010).
[31]V. Baranau and U. Tallarek, Soft Matter **10**, 3826 (2014).
[32]J. Mościński, M. Bargieł, Z. A. Rycerz, and P. W. M. Jacobs, Mol. Simul. **3**, 201 (1989).
[33]A. Bezrukov, M. Bargieł, and D. Stoyan, Part. Part. Syst. Charact. **19**, 111 (2002).
[34]B. D. Lubachevsky and F. H. Stillinger, J. Stat. Phys. **60**, 561 (1990).
[35]B. D. Lubachevsky, J. Comput. Phys. **94**, 255 (1991).
[36]V. Baranau, D. Hlushkou, S. Khirevich, and U. Tallarek, Soft Matter **9**, 3361 (2013); V. Baranau, PackingGeneration project (2013), https://code.google.com/p/packing-generation/.
[37]Y. Jiao, F. H. Stillinger, and S. Torquato, J. Appl. Phys. **109**, 013508 (2011).
[38]I. Biazzo, F. Caltagirone, G. Parisi, and F. Zamponi, Phys. Rev. Lett. **102**, 195701 (2009).
[39]Z. W. Salsburg and W. W. Wood, J. Chem. Phys. **37**, 798 (1962).
[40]L. Filion, M. Hermes, R. Ni, and M. Dijkstra, J. Chem. Phys. **133**, 4115 (2010).
[41]E. Sanz, C. Valeriani, E. Zaccarelli, W. C. K. Poon, P. N. Pusey, and M. E. Cates, Phys. Rev. Lett. **106**, 215701 (2011).
[42]C. Valeriani, E. Sanz, E. Zaccarelli, W. C. K. Poon, M. E. Cates, and P. N. Pusey, J. Phys.: Condens. Matter **23**, 194117 (2011).
[43]M. Pica Ciamarra, M. Nicodemi, and A. Coniglio, Soft Matter **6**, 2871 (2010).
[44]R. Ni, M. A. Cohen Stuart, and M. Dijkstra, Nat. Commun. **4**, 2704 (2013).